Chapter 7
Theory of Nucleation and Glass Formation

Kenneth F. Kelton

1 Introduction

Almost all first-order phase transformations are initiated by a process of nucleation, where small regions with an order parameter characterizing the new phase stochastically form [1]. In addition to the fundamental interest in this process, nucleation is of extreme practical importance. An ability to control nucleation is central to grain refinement [2], glass formation [3, 4], and the production of glass ceramics [5]. In addition, nucleation control is essential in the pharmaceutical [6, 7] and food [8, 9] industries, and it can play a vital role in biological systems [10] and in medical diseases [11].

A central feature of nucleation processes is the existence of a nucleation barrier. This was first evident in a set of experiments by Fahrenheit, who noted that liquid water could be maintained in a supercooled state (i.e., below the melting temperature) for long periods of time without crystallizing [12]. Turnbull was the first to observe this in liquid metals and showed that the amount of supercooling can be quite large, up to one third of the melting temperature in liquid mercury, for example [13]. Such dramatic supercooling in a liquid metal was surprising given the similarity in the densities of metallic liquids and crystals and their similar coordination numbers. It is now recognized that all metallic liquids can be deeply undercooled, typically to approximately 20% of their liquidus temperatures [1].

Nucleation can be either homogeneous or heterogeneous. Homogeneous nucleation is the more fundamental of the two types, occurring randomly in space and time. Heterogeneous nucleation is more common, occurring at specific sites in the initial phase. Even though it is less common, studies of homogeneous nucleation are possible under the right conditions. This chapter will focus on homogeneous

K. F. Kelton (✉)
Washington University in St. Louis, St. Louis, MO, USA
e-mail: kfk@wustl.edu

© The Minerals, Metals & Materials Society 2022

H.-J. Fecht, M. Mohr (eds.), *Metallurgy in Space*, The Minerals, Metals & Materials Series, https://doi.org/10.1007/978-3-030-89784-0_7

nucleation, review some experimental data in liquids and glasses, and discuss models for nucleation. A discussion of heterogeneous nucleation can be found elsewhere [1]. Computer simulations are increasingly valuable for enabling a microscopic investigation of nucleation processes and will also be briefly discussed. Of particular interest for this book are studies of nucleation under microgravity conditions. A brief discussion of these for protein, colloidal, and metallic liquids is presented. Finally the role of nucleation in glass formation is very briefly described.

2 Nucleation Theories

The classical nucleation theory (CNT) is most commonly used to analyze nucleation data, but it has several shortcomings. The most important of these are discussed in this section and more advanced theories that address them are presented. But, first, we turn to a discussion of CNT and its development.

2.1 Classical Nucleation Theory (CNT)

The thermodynamic formulation of CNT is due to J. W. Gibbs [14]. Assuming that the nucleation barrier arises from the energy required to create an interface between the initial phase and a small cluster of the new phase, he showed that the minimum amount of work required to form a spherical cluster of n atoms of the new phase, $W(n)$, is

$$W(n) = n\Delta\mu + \kappa n^{2/3}\sigma, \tag{7.1}$$

where $\Delta\mu$ is the difference in chemical potential between the original and the final phase, σ is the interfacial free energy between the nucleating cluster and the original phase, κ is a geometrical factor equal to $(4\pi)^{1/3}(3\overline{v})^{2/3}$, and $\overline{v}$ is the molecular volume. The work can also be expressed in terms of the cluster radius, r:

$$W(r) = \frac{4}{3}\pi r^3 \Delta g + 4\pi r^2 \sigma, \tag{7.2}$$

where $\Delta g = \Delta\mu/\overline{v}$. The work of cluster formation as a function of cluster size, n, is shown in Fig. 7.1a. For small clusters, $W(n)$ increases with increasing size but goes through a maximum, $W(n^*) = W^*$, at a critical cluster size n^*, beyond which it decreases with increasing size. As indicated, clusters smaller than n^* are on average dissolving, and those larger than n^* are on average growing. Nucleation is dominated by the time required for clusters to diffuse (in cluster size space) through a critical region that is located k_BT less than W^*, where k_B is the Boltzmann constant and T is the temperature in absolute units.

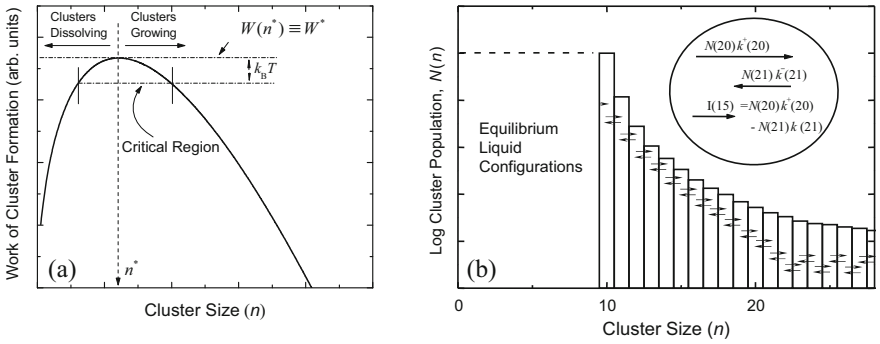

Fig. 7.1 (**a**) Work of cluster formation as a function of the number of molecules in the cluster, n, showing the critical size, n^*, and the critical region. (**b**) A histogram of the cluster population as a function of the number of molecules in a cluster, n. (Adapted from Ref. [1], copyright (2010), with permission from Elsevier)

The critical radius, r^*, is found by differentiating $W(r)$ with respect to the radius and setting that equal to zero, giving $r^* = 2\sigma/|\Delta g|$. The corresponding number of molecules in the critical cluster is $n^* = [32\pi/(3\overline{v})](\sigma/|\Delta g|)^3$. The critical work of cluster formation is obtained by substituting r^* into Eq. (7.2), giving

$$W^* = \frac{16\pi}{3}\frac{\sigma^3}{|\Delta g|^2} \tag{7.3}$$

Gibbs assumed that the nucleation rate is proportional to the probability of having a fluctuation that gives a cluster of the new phase containing n^* molecules, i.e., $\propto \exp(-W^*/k_B T)$. The computation of the proportionality constant requires a kinetic model that describes the rate that clusters evolve in size. Following an approach used in chemical kinetics, Volmer and Weber [15] assumed that this occurs by a series of bi-molecular reactions with single molecular attachment or detachment at each step, as illustrated in Fig. 7.1b. The nucleation rate is the flux past a given size and is in general time dependent:

$$I_{n,t} = N_{n,t}k_n^+ - N_{n+1,t}k_{n+1}^-. \tag{7.4}$$

Assuming, however, that the cluster distribution is time invariant, Becker and Döring [16] obtained an expression for the steady-state nucleation rate per mole:

$$I^{st} = k_{n*}^+ \left(\frac{|\Delta\mu|}{6\pi k_B T n^*}\right) N_A \exp\left(-\frac{W^*}{k_B T}\right) = k_{n*}^+ Z N_A \exp\left(-\frac{W^*}{k_B T}\right), \tag{7.5}$$

where N_A is Avogadro's number and Z is the Zeldovich factor. These equations were developed for gas condensation, for which k_{n*}^+ could be computed from molecular dynamics. Turnbull and Fischer were the first to apply them to nucleation from a

liquid by assuming that the kinetics of attachment were determined by the diffusion coefficient in the original phase [17], giving

$$I^s = \frac{24D(n^*)^{2/3}N_A}{\lambda^2} Z \exp\left(-\frac{W^*}{k_B T}\right) = A^* \exp\left(-\frac{W^*}{k_B T}\right). \quad (7.6)$$

The development of CNT assumes that the interface between the nucleating cluster and the original liquid or glass phase is sharp. The first suggestion that this might not be correct came from experimental studies of the nucleation rate in liquid mercury [13], where the pre-factor measured from fits to the data was seven orders of magnitude larger than the value calculated from Eq. (7.6). These were brought into agreement by assuming that the interfacial free energy, σ_{ls}, increased with temperature. Since a free energy should decrease, not increase, with increasing temperature due to the entropy term, Turnbull argued that there must be a sizable entropy deficit due to ordering in the liquid in front of the advancing interface. This indicates that the interface is then diffuse, rather than sharp. As discussed next, more sophisticated theories of nucleation support this conclusion.

2.2 *Density Functional Theory (DFT)*

DFT is based on a position-dependent order parameter description of the original and nucleating phases. The density is a good order parameter for gas condensation, since the densities of the two phases are very different. However, an order parameter that takes account of local symmetry is a better one for a liquid/glass to crystal transition. The work of cluster formation is expressed as a functional (i.e., a function of a function) of the chosen order parameter. By setting the derivative of the work with respect to the order parameter equal to zero, the critical fluctuation of the order parameter is obtained. This is analogous to the critical size in CNT. A more in-depth discussion may be found elsewhere (Chapter 4 in Ref. [1]).

There have been many proposed DFT formulations of the work of cluster formation (see Chapter 4 in Ref. [1]). Gránásy tested these for nucleation in liquids [18] and glasses [19], finding that the semi-empirical density functional approximation (SDFA) fit the data best. This model is based on a single non-conserved structural order parameter, M, which is equal to 1 in the macroscopic crystal phase and zero in the liquid phase [20]. Two key predictions from this theory are as follows: (i) the interface is diffuse, not sharp, and (ii) the order parameter becomes much less than the expected value of 1, even in the center of the cluster, as the departure from equilibrium is increased (i.e., increased supercooling for crystallization from the liquid). These points are illustrated in Fig. 7.2a, for the order parameter as a function of scaled distance for three different scaled critical sizes, which correspond to three values of $\tilde{\Delta}$, a scaled dimensionless free energy difference between the liquid and the solid.

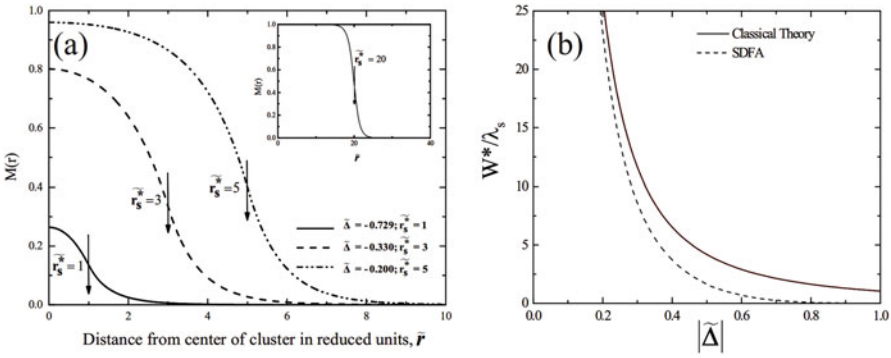

Fig. 7.2 (**a**) The order parameter, *M*, as a function of the scaled distance from the center of the cluster, measured in reduced units. (**b**) The scaled work of formation as a function of the scaled driving free energy. (Reprinted with permission from Ref. [20], copyright (1994), American Institute of Physics)

As for CNT, the values of $\widetilde{\Delta}$ become more negative, and the critical sizes decrease with increased departure from equilibrium, with the order parameter systematically decreasing in the center of the cluster. For large departures from equilibrium, the difference between the order parameter in the cluster and in the liquid is very small, indicating that the structural order in the liquid and the nucleating phase is similar. Close to equilibrium, shown in the inset, the order parameter is the same as for the macroscopic crystal, although it should be noted that the interface remains diffuse.

The predictions of the work of critical cluster formation behave similarly as a function of $\widetilde{\Delta}$. As shown in Fig. 7.2b, the critical work from the SDFA, scaled to the curvature of the free energy curve for the solid phase, (W^*/λ_s), approaches the value for that calculated from CNT for small magnitudes of $\widetilde{\Delta}$, i.e., close to equilibrium. The value from SDFA becomes less than the value from CNT with increasing magnitude of $\widetilde{\Delta}$, approaching zero at large departures from equilibrium.

2.3 Diffuse Interface Theory (DIT) of Nucleation

While density functional theories give quantitative predictions for the profile of the order parameter, their use for analyzing nucleation experimental data is not straightforward since many of the parameters needed are poorly known or not known at all. The diffuse interface theory (DIT) [21–23] offers a phenomenological thermodynamic approach that can be more readily used. In contrast with the CNT, the DIT explicitly assumes that the interface is diffuse, in agreement with predictions from DFT theories (Sect. 2.2) and computer simulations (Sect. 3). Based on the DFT studies, the profile of the Gibbs free energy should qualitatively have the form shown in Fig. 7.3a, with a maximum in the interfacial region.

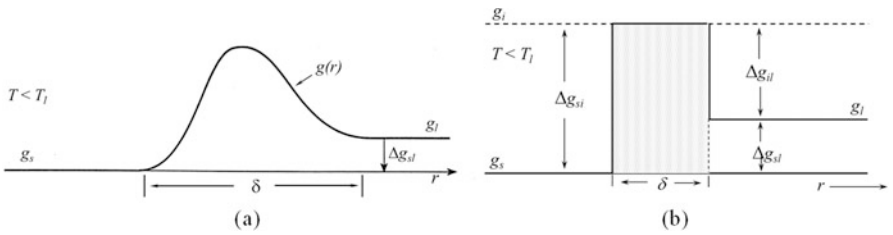

Fig. 7.3 (**a**) The qualitative profile of the Gibbs free energy density as a function of distance through the interfacial region. (**b**) The simplified profile assumed within the DIT. (Adapted from Ref. [21], copyright (1994), with permission from Elsevier)

As shown in Fig. 7.3b, within the DIT this profile can be approximated as a step function having a width δ, which corresponds to the width of the interface. The interfacial width reflects the difference between the profile of the enthalpy and the entropy on transitioning through the interface [24]. Assuming a spherical cluster, the work of cluster formation is

$$W = \int_0^\infty (\Delta h - T\Delta s) 4\pi r^2 dr \tag{7.7}$$

where $\Delta h = N(r)[H(r) - H_1]$ and $\Delta s = N(r)[S(r) - S_1]$, $N(r)$ is the local molecular number density, and $H(r)$ and $S(r)$ are the molecular enthalpy and entropy; the subscript one refers to the parent phase. For clusters with a radius that is significantly larger than the interfacial width, $\delta \cong R_S - R_H$, where R_H and R_S are the midpoints of the enthalpy and entropy profiles on traversing through the interface. It follows that $\Delta h \cong \Delta h_0[1 - \theta(r - R_H)]$ and $\Delta s \cong \Delta s_0[1 - \theta(r - R_S)]$, where θ represents the step function approximation in Fig. 7.3b. The work of cluster formation is

$$W = \frac{4\pi}{3}\left(R_H^3 \Delta h_0 - R_S^3 T\Delta s_0\right) \tag{7.8}$$

and the area enclosed between the Δh and $T\Delta s$ curves is proportional to the interfacial free energy. Using $\delta \cong R_S - R_H$ and maximizing the work of cluster formation with respect to R_S, the critical size, R_S^*, and the critical work of cluster formation, W^*, can be obtained:

$$R_S^* = \frac{\delta\Delta h_0 + \delta\sqrt{\Delta h_0 T\Delta s_0}}{\Delta h_0 - T\Delta s_0} \quad \text{and} \quad W^* = -\frac{4\pi}{3}\delta^3 \Delta g_o \psi \tag{7.9}$$

where $\Delta g_o = \Delta h_o - T\Delta s_o$, $\psi = 2(1+q)\zeta^{-3} - (3+2q)\zeta^{-2} + \zeta^{-1}$, $q = (1-\zeta)^{1/2}$, and $\zeta = \Delta g_o/\Delta h_o$. The critical work of formation can be written in a more compact form as [25]

$$W^* = -\frac{\frac{4\pi}{3}\delta^3 \Delta h_0 T \Delta s_0}{\Delta h_0 + T\Delta s_0 - 2\sqrt{\Delta h_0 T \Delta s_0}}. \tag{7.10}$$

A key result of the DIT model is the confirmation that a positive temperature dependence of the interfacial free energy indicates that the interface of the nucleating cluster is more ordered than the liquid or glass parent phase [21].

2.4 Composition Effects on Nucleation

The theories discussed in Sects. 2.1, 2.2, and 2.3 apply to nucleation processes in which the chemical compositions of the initial and final phases are the same. This is true for only a limited number of cases. If the diffusion rates are sufficiently fast in undercooled liquids, only interfacial processes need be considered. It is then reasonable to expect that the steady-state nucleation rate for a binary system (A, B) will be

$$I^s_{a,b} = A^*_{a,b} \exp\left(-\frac{W^*_{a,b}}{k_B T}\right), \tag{7.11}$$

where $W^*_{a,b}$ is the reversible work of formation of a cluster of critical size n^*, composed of a^* molecules of A and b^* molecules of B, and $A^*_{a,b}$ is the pre-factor. Assuming an effective interfacial free energy, σ, for a sharp interface between the nucleating cluster and the parent phase, $W_{a,\,b}$ is (approximately)

$$W_{a,b} = a\delta g_A + b\delta g_B + \zeta\sigma(a\overline{v}_A + b\overline{v}_B)^{2/3} \tag{7.12}$$

where δg_A and δg_B are the changes in the Gibbs free energy per atom for A and B, ζ is a geometric factor (which is $(36\pi)^{1/3}$ for spherical clusters), and $\overline{v}_A$ and are the molecular volumes of A and B atoms, respectively. Reiss showed [26] that the pre-factor, $A^*_{a,b}$ is a function of the composition of A and B in the liquid, their atomic mobility at the interface, and the two mutually orthogonal curvatures of $W_{a,b}$ at the saddle point, P and Q. Assuming that the forward and backward rate constants have a similar form to those in the CNT and that the cluster composition corresponds to the maximum driving free energy (corresponding to a saddle point in the free energy as a function of the cluster number and concentration), he obtained the following expression for the steady-state nucleation rate:

$$I^s = k^+_{a^*,b^*}\sqrt{P/Q}N^{eq}_{a^*,b^*}, \tag{7.13}$$

where the equilibrium number of clusters at the critical size in terms of Avogadro's number of single molecules, N^0_A and N^0_B, is [27]

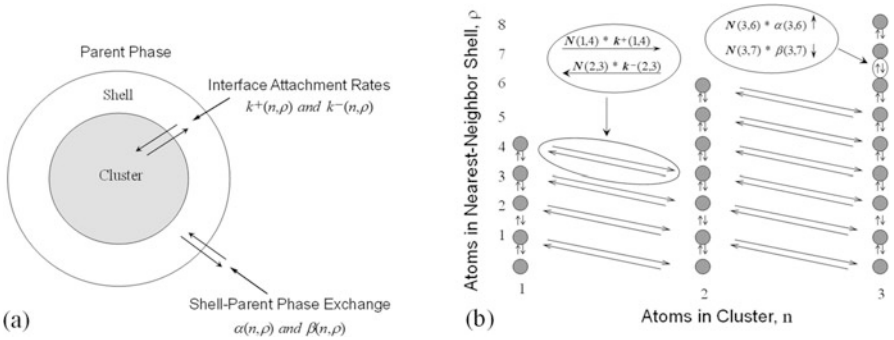

Fig. 7.4 (**a**) Schematic illustration of the fundamental features of the coupled-flux model, showing the interfacial fluxes and those between the shell and parent phase. (**b**) Schematic illustration of the kinetic processes in the coupled-flux model, shown here up to a cluster size of 3. Motion between the shell and the parent phase, changing the shell composition, occurs along the vertical axes, while interfacial attachment occurs along the horizontal and diagonal lines. The upper cutoff of the vertical axis corresponds to a complete filling of the shell region of a cluster of size n. (Adapted from Ref. [34], copyright (2000), with permission from Elsevier)

$$N_{a,b}^{\mathrm{eq}} = \left(N_A^0\right)^{N_A^0/\left(N_A^0+N_B^0\right)} \left(N_B^0\right)^{N_B^0/\left(N_A^0+N_B^0\right)} \exp\left(-\frac{W_{a,b}}{k_{\mathrm{B}}T}\right). \tag{7.14}$$

The effect of chemical composition is reflected in changes in the driving free energy, interfacial free energy, and the atomic mobility. Several refined treatments have been offered to deal with shortcomings in Reiss development [28–30]. Wu offered the most complete solution for binary nucleation by mapping nucleation onto a one-component system [27]. His approach can also be extended to more than two component systems. A more detailed discussion of interface controlled multicomponent nucleation can be found elsewhere [1].

If the diffusion and interface kinetics are comparable, the stochastic fluxes for diffusion in cluster space and diffusion in the real space of the parent phase become coupled, which can have a strong influence on nucleation in cases like solid-state transformations, precipitation, and crystallization from the liquid phase, if stirring is minimized such as in a microgravity environment. To understand this, it is easiest to think about precipitation of a pure phase from solute atoms in a solution. Following an approach first suggested by Russell [31], the coupled fluxes can be treated by focusing attention on three regions: the cluster, the immediate neighborhood around the cluster, and the parent phase (Fig. 7.4a). The number of atoms in the cluster, n, and the number in the cluster neighborhood, ρ, must both be considered. Assuming that the number of atoms in the clusters and their nearest-neighbor shells occur by the gain or loss of a single atom at a time, the rate kinetics are described within a two-dimensional (n,ρ) space (Fig. 7.4b). Since only the nearest-neighbor shell is considered, the upper limit on ρ (p^m) increases with cluster size n, $p^m \approx 4n^{2/3}$, giving the staircase appearance in Fig. 7.4b.

The equilibrium cluster distribution in the coupled-flux model is

$$N(n,\rho) = N_{\mathrm{o}} \exp\left(-\frac{W_{\mathrm{n}}}{k_{\mathrm{B}}T}\right) P\{\rho\}, \tag{7.15}$$

where N_{o} is the number of solute atoms per unit volume in the initial phase distributed among the number of possible sites (N_{S}), W_{n} is the work of cluster formation, and $P\{\rho\}$ is the probability for having ρ solute atoms in the nearest-neighbor shell around the cluster. For simplicity, the work of cluster formation is taken to be the same as in the classical theory. From Fig. 7.4b, the differential equation that describe the rate of change of the cluster distribution is

$$\begin{aligned}\frac{\partial N(n,\rho,t)}{\partial t} &= \alpha(n,\rho-1)N(n,\rho-1,t) - [\alpha(n,\rho)+\beta(n,\rho)]N(n,\rho,t) \\ &+\beta(n,\rho+1)N(n,\rho+1,t) + k^{+}(n-1,\rho+1)N(n-1,\rho+1,t) \\ &+k^{-}(n+1,\rho-1)N(n+1,\rho-1,t) - [k^{+}(n,\rho)+k^{-}(n,\rho)]N(n,\rho,t).\end{aligned} \tag{7.16}$$

This is a natural extension of the differential equation in CNT that describes cluster growth in size space. The interfacial attachment and detachment rates as well as the rates controlling the parent/shell exchanges are discussed in Chapter 5 of Ref. [1].

The steady-state nucleation rate obtained from a numerical solution of Eq. (7.16) as a function of the ratio of the effective long-range diffusion coefficient, ξD, to the effective diffusion coefficient governing interfacial attachment, D_{i}, is shown in Fig. 7.5. (The constant ξ is introduced to take proper account of the average diffusion distance for an atom to leave the shell and return to the parent phase. Its value is determined by setting the cluster growth rate for large clusters in coupled-flux nucleation equal to the known diffusive macroscopic growth rate.) For $\xi D < D_{\mathrm{i}}$, the steady-state rate scales linearly with the ratio of rates. With increasing values of the ratio, the coupled-flux nucleation rate asymptotically approaches the CNT value (shown by the dashed line), reflecting the crossover from diffusion limited to interface-limited nucleation. Predictions from the coupled-flux model have been shown to be in much better agreement with nucleation data for oxygen precipitation in silicon than are CNT calculations [32], and they agree with the results from a kinetic Monte Carlo simulation [33].

3 Computer Modeling Studies of Nucleation

Computer models for nucleation are becoming increasingly more important for probing the underlying processes involved in nucleation. For example, Monte Carlo studies of Ising models have demonstrated the stochastic nature of nucleation [35]. Ising models have also been useful in studies of the pre-factor, A^{*}. Fits to the simulation data, for example, show that A^{*} is several orders of magnitude smaller than expected from CNT and is a strong function of cluster size [28, 36]. A more extended discussion of these early results can be found elsewhere [1].

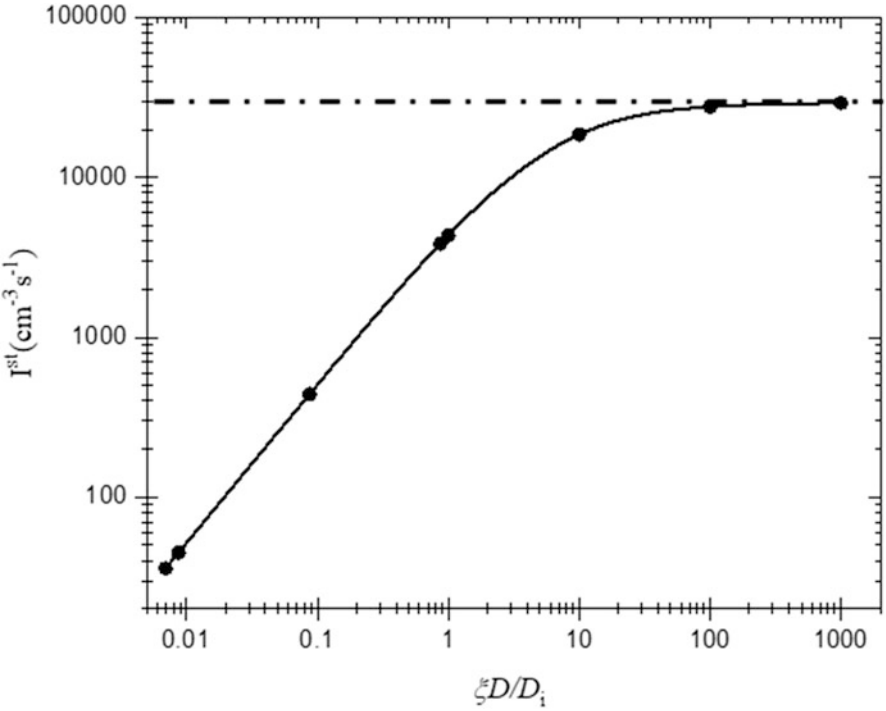

Fig. 7.5 The steady-state nucleation rate computed from the coupled-flux differential equations as a function of the ratio of the effective diffusion rate in the parent phase, ξD, to an effective diffusion rate governing interfacial attachment, D_i. The dashed line corresponds to the nucleation rate from CNT multiplied by $x^{2/3}$, where x is the atom fraction of solute ($x = N_o/N_S$). (Adapted from Ref. [34], copyright (2000), with permission from Elsevier)

Molecular dynamics (MD) studies have demonstrated the existence of a nucleation barrier [37] and have identified the critical sizes [38]. However, the ensemble sizes in these early simulations consisted of a few thousand to a few ten thousand atoms. Within the past decade, the increase in computer speed and the amount of accessible memory have greatly expanded the ensemble sizes, some now containing up to a billion atoms. The MD simulations have provided new insight into the validity of some of the key assumptions in the development of the CNT and have identified new features of nucleation that have not yet been incorporated into analytical models. Most of these are classical MD simulations, which use model potentials that may not capture all of the features of the actual atomic interactions and the structural development. First-principle (ab initio) calculations are not hindered by these problems, but the ensemble sizes that can be studied are very limited. Ab initio calculations are most useful for studies of small clusters of atoms, identifying structural and chemical ordering more accurately than classical MD studies.

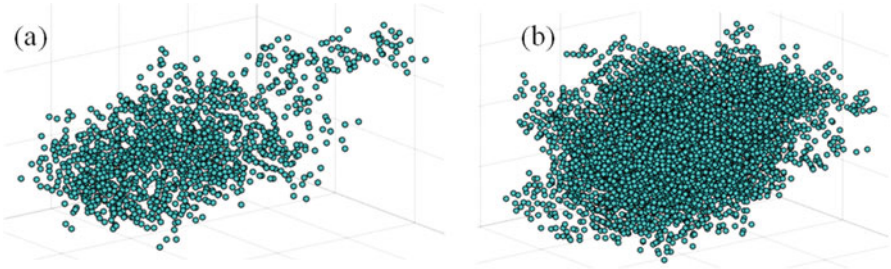

Fig. 7.6 (**a**) 1226 atom $Al_{20}Ni_{60}Zr_{20}$ bcc cluster at 1016 K. (**b**) 4330 atom $Al_{20}Ni_{60}Zr_{20}$ bcc cluster at 996 K

The properties of the nucleating clusters are critically important for developing a quantitative understanding of nucleation. Monte Carlo studies of a 100-atom cluster suggested that the clusters that formed in an Ar vapor are diffuse [39]. This is dramatically evident in recent MD calculations. Figure 7.6a shows a bcc crystal cluster of 1226 atoms that has nucleated in a supercooled liquid of $Al_{20}Ni_{60}Zr_{20}$, for an ensemble size of 1 million atoms [40]. The cluster is clearly not compact nor spherical, as assumed in the CNT, although it approximates this more closely as the cluster size increases (Fig. 7.6b). In all cases, however, the interface is diffuse. A study of a large number of clusters in the ensemble shows that both the density and the bcc order parameter decay on transitioning from the center of the cluster to the cluster boundary, in agreement with the density functional and diffuse interface models for nucleation discussed in Sect. 2.

As will be discussed in Sect. 4, experimental studies have confirmed Frank's hypothesis [41] that icosahedral short-range order (ISRO) develops in many supercooled transition metal alloy liquids and that this order couples to the nucleation barrier, making it more difficult to nucleate crystallographic phases. Ab initio MD studies have shown that the degree of ISRO is more prominent for bcc forming liquids and less so in fcc and hcp forming liquids, possibly because icosahedral disclination line defects are more easily incorporated into bcc environments [42]. While initially growing in the supercooled bcc forming liquid, the ISRO begins to decrease upon approaching the nucleation temperature, replaced by local bcc ordering [43, 44]. Regions of bcc ordering also appear in the initial nucleation of Zn and Pb, before crystallizing to the hcp or fcc structures, respectively [45]. All of the models discussed in Sect. 2 assume that nucleation can occur anywhere within the liquid. These MD results suggest that nucleation is more complicated than that. The results are in agreement with the proposed explanation of the experimental studies in $Ti_{39.5}Zr_{39.5}Ni_{21}$, i.e., that regions of order in the liquid catalyze the nucleation of the crystal phases [46]. They also suggest that nucleation is a coupled process, with orientational ordering occurring prior to density ordering, as was proposed by Tanaka and co-workers [47, 48]. An MD result indicates that chemical ordering can also catalyze nucleation [49], as predicted earlier [50]. The result that nuclei initially have a bcc orientational order before changing to the expected crystal

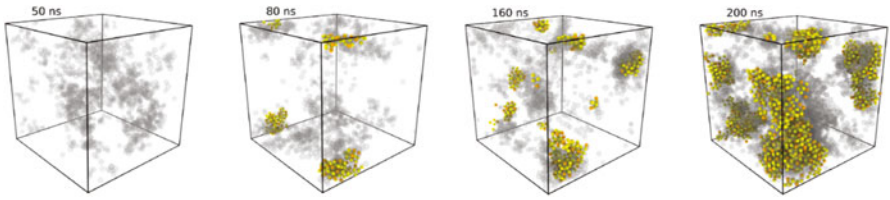

Fig. 7.7 The correlation between the slow regions of dynamical heterogeneities (gray regions) with the formation of crystal nuclei (colored spheres) for several times at 837 K. (Reprinted with permission from Ref. [53], copyright (2019), American Physical Society)

structure indicates that the nucleation pathway is more complicated than assumed; a similar case was recently identified in a silicate glass, where the first phase to nucleate had a chemical composition different from that of the crystallizing phase [51]. A billion atom MD simulation of pure Fe indicated that nucleation proceeds in two stages where satellite nuclei form in the region surrounding the initial nuclei [52]. This has not been reported in other MD simulations; however, so further investigation is called for to understand why this might be the case.

Recent MD studies also suggest an additional role for ISRO in the kinetics of nucleation in metallic liquids. Liquids are known to be characterized by heterogeneous structures and dynamics. Many MD calculations have shown that local regions with icosahedral order are also dynamically slow [54]. The development of these dynamical heterogeneities has been argued to underlie the breakdown of the Stokes-Einstein relation [55] and lead to the glass transition. As illustrated in Fig. 7.7, MD studies also suggest that these are the sites where nucleation preferentially occurs. The development of dynamically slow regions with local icosahedral order occurs after 20 ns at 837 K; subsequent nucleation and growth of the Cu_5Zr phase preferentially occur in these regions [56].

There have been a few studies of the agreement between the predicted nucleation rate and computer results, and the results have been varied. A study of the Lennard-Jones liquid, for example, found that nucleation proceeds along multiple pathways around the minimum free energy path and that in addition to size, the shape and structure of growing clusters play an important role [57], features that are not commensurate with CNT. However, a later study of liquid Al showed good agreement with CNT, particularly the time lag for nucleation [58]. A later MD study of nucleation in liquid Al found that the nucleation times followed a Poisson distribution, in agreement with the stochastic model for nucleation in CNT. They also found agreement to within one order of magnitude between the simulation results and CNT predictions, although this required using the pre-term and the interfacial free energy as fitting parameters [59]. A recent MD study of nucleation in a barium sulfide (BaS) liquid found agreement to within an order of magnitude with predictions from CNT, using only the interfacial free energy as a fitting parameter [60]. Similar results were obtained for nucleation in a $Ni_{50}Ti_{50}$ liquid [61]. So, despite the problems with CNT identified earlier, it seems that it remains a reasonable phenomenological framework

for describing homogeneous polymorphic nucleation, if the interfacial free energy is taken as a fitting parameter.

4 Ground-Based Studies of Nucleation in Metallic Liquids

The earliest attempts to study homogeneous nucleation in liquids used methods to isolate impurities that would cause heterogeneous nucleation (see Ref. [1], Chapter 7). The samples were dispersed into fine droplets either in a medium on or a surface so that some of the droplets would be free of impurities. The maximum supercooling observed was then attributed to homogeneous nucleation in those droplets.

Recently, levitation techniques have been developed that allow single macroscopic droplets to be repeatedly processed in a containerless environment. The most common of these are electromagnetic levitation and electrostatic levitation, which are discussed in Chaps. 3, 5, 8, 10, and 12 in this book. A statistical analysis of many measurements of the maximum supercooling from a single droplet in a containerless, high-vacuum environment can in principle allow studies of the type of nucleation (heterogeneous or homogeneous) and the different nucleation barriers for the nucleating phases. It is assumed that due to the rapid growth rates at high temperatures, one nucleation event leads to crystallization of the droplet, and the solidification is essentially adiabatic [62, 63]. The probability density for one nucleation event as a function of temperature at a constant cooling rate, Q, is [1, 64]

$$P(1;T) = \frac{I^{\mathrm{st}}(T)V}{Q} \exp\left(-\frac{V}{Q} \int_{T_{\min}}^{T_{\ell}} I^{\mathrm{st}}(T)\mathrm{d}T \right), \tag{7.17}$$

where V is the volume of the droplet, I^{st} is the steady-state nucleation rate, T_{ℓ} is the liquidus temperature (the melting temperature for a pure liquid), and $T_{\min}$ is the maximum supercooling temperature. The shape of the distribution is sensitive to the temperature dependence of the nucleation pre-factor and the nucleation barrier. As the magnitude of the pre-factor increases, the distribution becomes narrower and less skewed toward lower temperatures (smaller third moment). The validity of the Skripov method was examined by measuring the supercooling distribution in zirconium liquid samples of three different purities [62] and by Monte Carlo calculations [63].

As discussed in the introduction, the ability to significantly supercool liquid metals, indicating the presence of a significant nucleation barrier, came as a surprise when it was first reported. Before Turnbull's studies of dispersed droplets, this had not been possible. Although he recognized that the failure of previous attempts to supercool was likely due to heterogeneous nucleation, this was not widely regarded as the reason. Instead, the similarity in the densities and coordination numbers of the

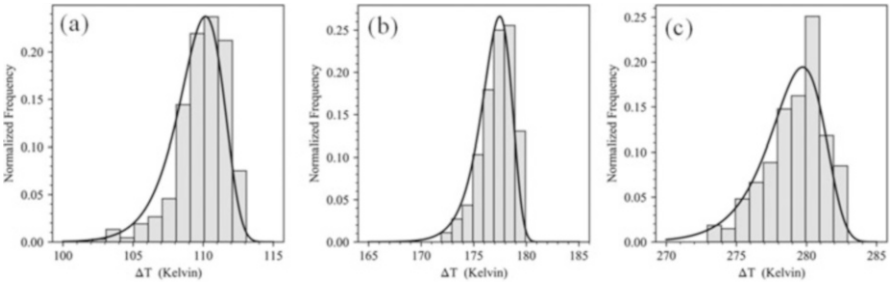

Fig. 7.8 (**a**) The histogram of maximum supercooling values for $Ti_{39.5}Zr_{39.5}Ni_{21}$, (**b**) $Ti_{40}Zr_{40}Ni_{30}$, and (**c**) $Zr_{80}Pt_{20}$. The solid line shows the fit to Eq. (7.17). (Reprinted with permission from Ref. [67] copyright (2019), American Institute of Physics)

Table 7.1 Fit values for nucleation parameters

Liquid	A^* $(m^3s)^{-1}$	W^*/k_BT	σ (J/m^2)
$Ti_{39.5}Zr_{39.5}Ni_{21}$	2.74×10^{25}	37.18	0.057
$Ti_{40}Zr_{30}Ni_{30}$	4.85×10^{39}	70.54	0.114
$Zr_{80}Pt_{20}$	8.76×10^{45}	84.17	0.134

Data from Ref. [67]

liquids and corresponding crystal phases led many to believe that the phases have similar local atomic order and hence the nucleation barrier should be small. Frank proposed that the local structure of the liquid was dominated by icosahedral order, which like close-packed crystal phases has a coordination number of 12 and a similar density [41]. X-ray scattering studies have demonstrated that transition metal liquids do indeed contain a significant amount of icosahedral short-range order (ISRO) [65]. This order was linked to the nucleation barrier in a liquid that nucleated a metastable icosahedral quasicrystal phase [46], a non-translationally ordered phase with extended icosahedral order [66]. As a further investigation into this problem, the Skripov method was recently employed to analyze maximum supercooling data for metallic liquids that contain significant ISRO but nucleate different phases, some of which have ISRO and some do not [67]. The alloy liquids investigated were $Ti_{39.5}Zr_{39.5}Ni_{21}$, which nucleates the icosahedral quasicrystal; $Ti_{40}Zr_{40}Ni_{30}$, which forms the C14 Laves phase (a poly-tetrahedral crystal phase with local order similar to that of the icosahedral quasicrystal); and $Zr_{80}Pt_{20}$, which nucleates a phase mixture of Zr_5Pt_3 and βZr, both phases lacking icosahedral or poly-tetrahedral order. Several hundred supercooling studies were made for each of the three alloys. The resulting distributions and the fits to Eq. (7.17) are shown in Fig. 7.8. In all cases the fits were good, with p-values greater than 0.999.

The values for the nucleation pre-factor, A^*; the work of critical cluster formation, W^*; and the value for the interfacial free energy, σ, obtained from the fits are listed in Table 7.1. A^* increases with decreasing icosahedral local order of the nucleating crystal phases, as do the work of cluster formation and consequently the interfacial free energy. This is consistent with Frank's hypothesis. The smallest value for A^* in the quasicrystal-forming liquid suggests that the local regions of icosahedral order in

the liquid catalyze the nucleation of the ordered phase. This is consistent with the computer modeling studies shown in Fig. 7.7 and with conclusions from X-ray scattering studies [46]. It could also be consistent with a proposal by Tanaka that nucleation proceeds in stages instead of the one-step nucleation approach in the classical theory [68]. In that case, the small nucleating region first undergoes spatial ordering (to ISRO in this case) and then densifies. As already mentioned, these multiple pathways for nucleation is an emerging topic of considerable interest

5 Nucleation in Metallic and Silicate Glasses

Nucleation has been studied extensively in the silicate glasses. Understanding and controlling crystal nucleation is essential in glass formation and is also important in the production of glass ceramics with the desired properties. Both the nucleation and growth rates have peaks as a function of temperature, although the quantitative function is different for the two rates. The two peaks are often significantly separated in temperature in silicate glasses, which allows the nucleation rate to be accurately measured using a two-step annealing method, in which samples of the glass are first annealed for different times at a temperature, T_N, where the nucleation rate is high, but the growth rate is low to produce a population of small nuclei. These nuclei are then grown to visible size by heating at a higher temperature, T_G, where the growth rate is large, but the nucleation rate is small. For steady-state nucleation, the number of nuclei produced at T_N should be a linear function of the annealing time, so the slope of the line fit through the data will equal the steady-state nucleation rate. However, as shown in Fig. 7.9a for a barium silicate glass, the observed behavior is quite different. For long annealing time, the nucleation rate eventually reaches the steady-state rate, but at shorter times, the rate is smaller. The extrapolation of the straight line to the time axis gives the induction time, θ, which provides a measure of the relaxation time of the cluster distribution inherited from high temperature to the steady-state distribution at T_N. This is an example of time-dependent nucleation, which is best described by the following expression [69]:

$$I_{n*,t} = I^{st}\left[1 + 2\sum_{m=1}^{\infty}(-1)^m \exp\left(-\frac{m^2 t}{\tau_K}\right)\right] \quad . \tag{7.18}$$

I^{st} is the steady-state nucleation rate. The Kashchiev transient time, τ_K, is related to the induction time, θ, by

$$\tau_K = -\frac{24 k_B T n^*}{\pi^2 k^+_{n*} \delta\mu} = \frac{6}{\pi^2}\theta. \tag{7.19}$$

Since θ scales inversely with k^+_{n*}, a more quantitative fit to glass nucleation data is possible than by using the diffusion coefficient or viscosity of the glass.

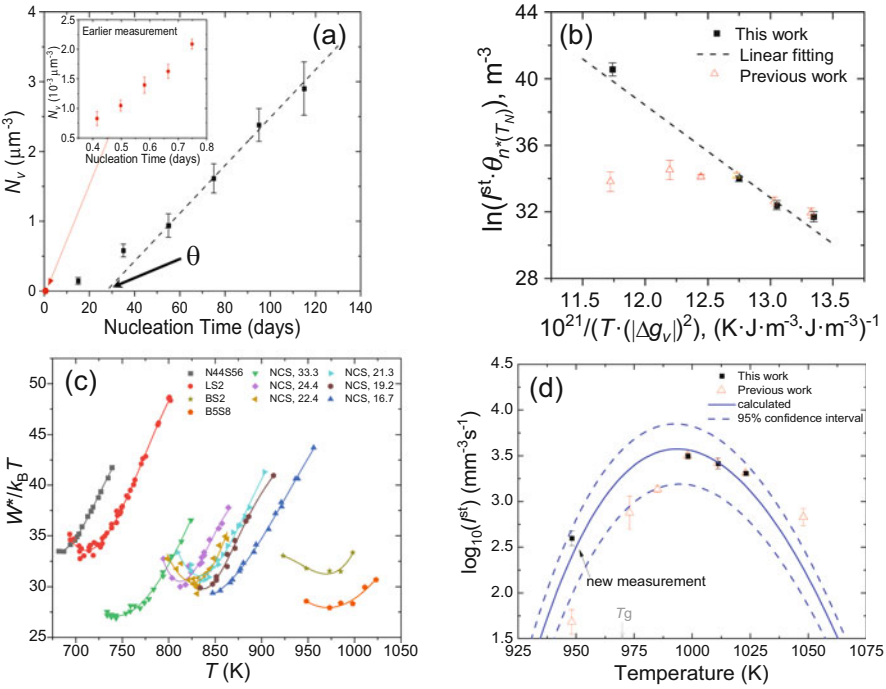

Fig. 7.9 (**a**) The number of nuclei per unit volume as a function of nucleation time at 948 K for a $5BaO{\cdot}8SiO_2$ glass; previously measured data [70] are shown in the inset. (**b**) A plot of $\ln(I^{st}\theta_{n^*(TN)})$ vs. $1/(T|\Delta g_v|^2$ for the $5BaO{\cdot}8SiO_2$ glass from the previously measured data [70] (red triangles) and the more recent data [71] (dark squares). The dashed line is the expected linear behavior. (**c**) The scaled nucleation barrier, W^*/k_BT, as a function of temperature for several silicate glasses, $44Na_2O{\cdot}56SiO_2$ (N44S56), $Li_2O{\cdot}2SiO_2$ (LS2), $BaO{\cdot}2SiO_2$ (BS2), $5BaO{\cdot}8SiO_2$ (B5S8), and $xNa_2O{\cdot}(50\text{-}x)CaO{\cdot}50SiO_2$ (NCS), where x values are 33.3, 24.4, 22.4, 21.3, 19.2, and 16.7 (see [71] for the data sources). The solid lines are guides to the eye. (**d**) The logarithm of the steady-state nucleation rate for a $5BaO{\cdot}8SiO_2$ glass. The CNT-predicted rate, based on fits to data obtained at temperatures higher than the peak temperature, is shown by the solid line. The previous data point (red triangle) at 948 K (corresponding to the inset in (**a**)) and the good agreement with the new data point at 948 K (black square). The dashed lines are the 95% confidence limits for the calculated curve. (From Ref. [71])

For over 40 years, it has been noted that below the peak nucleation temperature the measured nucleation rates in many silicate glasses lie below values expected from CNT. The CNT predicts that a plot of $\ln(I^{st}\theta_{n^*(TN)})$ as a function of $1/(T|\Delta g_v|^2)$ (where $\theta_{n^*(TN)}$ is the induction time measured for the critical size at the nucleation temperature and Δg_v is the driving free energy) should be linear when σ is a constant or when the relative change in σ as a function of temperature is smaller than the relative change in $|\Delta g_v|$. An example of this is shown in Fig. 7.9b for a $BaO{\cdot}2SiO_2$ glass. The plot is linear at high temperatures but becomes increasingly nonlinear at low temperatures. Further, the scaled critical work of cluster formation, W^*/k_BT, derived from the data should decrease monotonically with decreasing temperature.

As shown in Fig. 7.9c, however, for many silicate glasses, W^*/k_BT plateaus and even begins to increase at low temperatures. All of these results suggest a failure of CNT at low temperatures, where the glass is far from equilibrium.

Many explanations have been advanced to explain this anomalous behavior [72–75]. However, because the function for the number of nuclei produced as a function of time is self-similar at different times, the failure could be an experimental artifact caused by insufficient annealing time at T_N to reach the steady state [76]. As an example, the inset in Fig. 7.9a shows data taken for approximately 1 day of annealing. After approximately one half of a day of annealing, the number of nuclei appears to increase linearly with time, suggesting that the steady-state rate has been reached. These data were used to compute the work of cluster formation for this glass that is shown in Fig. 7.9c [70]. However, as shown by the more recent data (black data points) in Fig. 7.9a, the data in the insert has clearly not reached the steady state. Using the new data from Fig. 7.9a, there is no longer an anomalous behavior in a plot of $\ln(I^{st}\theta_{n^*(TN)})$ vs. $1/(T|\Delta g_v|^2$ (black data points in Fig. 7.9b) nor in the work of cluster formation [71]. Also, the steady-state nucleation data point at 748 K is now in good agreement with CNT predictions (Fig. 7.9d). Given the results for this glass, and the fact that all other silicate glasses show a similar anomalous behavior at low temperature, it is possible that all of the existing nucleation data for silicate glasses at temperatures below the peak are incorrect. As for the results discussed in Sect. 3, it appears that CNT remains quantitatively correct (but with a temperature-dependent interfacial free energy, consistent with a diffuse interface) even in cases where nucleation occurs far from equilibrium. Studies have also shown that the kinetic model of CNT appears to be quantitatively correct at these low temperatures [77, 78]. Therefore, if a breakdown of CNT does occur as suggested from the DFT calculations, it must be at even greater departures from equilibrium and may not be experimentally accessible.

Nucleation rate measurements in metallic glasses have been obtained from single-step annealing treatments [79] and from ultrafast heating and cooling studies [80, 81]. Two-step annealing studies are more difficult because of the overlap in the temperature ranges for nucleation and growth. The one result for the nucleation of an icosahedral phase in a $Zr_{59}Ti_3Cu_{20}Ni_8Al_{10}$ glass was consistent with predictions from CNT for time-dependent nucleation. Further, the interfacial free energy derived from the fit to that data was extremely small (0.01 ± 0.004 J/m^2), consistent with the observed icosahedral order in the glass.

6 Stirring Effects on Nucleation and Microgravity

On Earth, liquids are stirred by Marangoni and gravity-induced flow, which can mask some features of nucleation, such as the diffusion effects discussed in Sect. 2.4. Stirring effects are also important in the crystallization and aggregation of proteins [82] and industrial crystallization in the pharmaceutical industry [83]. To examine these effects, nucleation rate measurements have been made in stirred environments

on Earth and in the less stirred microgravity environment available on parabolic flights, the space shuttle, and most recently the International Space Station.

Most studies have been made for proteins [84] and colloids, with a smaller number of studies of inorganic liquids [85] [86]. The results are varied. Some studies have reported that shear flow decreases the nucleation rate [87], while others have found a considerable increase in the rate under stirring [88, 89]. One simulation of colloids with a screened repulsion suggest that the nucleation barrier increases as the square of the shear rate [90], and others offer evidence for a maximum nucleation rate with stirring [91, 92]. A recent extension of CNT gives good agreement with this disparate behavior. It accounts for the contribution of flow to the kinetics of interfacial attachment in the Volmer-Weber kinetic equations but also argues for a change in the work of cluster formation due to mechanical deformation of the nucleus due to the flow [93]. These two competing effects lead to a maximum in the nucleation rate and a quadratic dependence of the nucleation rate on stirring, in agreement with the simulation results. Studies in a microgravity environment allow the effect of stirring on the nucleation rate to be investigated. But, they also allow other features of the nucleation process that are otherwise masked by flow to be explored. Emerging key features are that nucleation involves a degree of self-organization that is dependent on geometric, kinetic, and structural factors and that it is described by multiple order parameters involving non-classical nucleation pathways. As already mentioned, similar results have resulted from studies of crystallization in silicate glasses.

There are fewer studies of the effect of stirring on metallic liquids. A study of nucleation in liquid Zr as a function of stirring in the MSL mission on Spacelab found no evidence of a change in the rate for flow rates between 5 and 43 cm/s, based on the maximum supercooling achieved prior to crystallization. Above 50 cm/s the supercooling was smaller, which was taken as evidence for cavitation-induced nucleation in the liquid [94]. The maximum supercooling of liquid $Al_{40}Ni_{60}$ was 70 K smaller in a microgravity environment than it was in ground-based experiments [95]. One possible explanation is that since a thin layer of Al_2O_3 forms on the surface of the Al, and since there is evidence that the liquid orders next to this layer [96, 97], the layer could catalyze nucleation, as in the case where the icosahedral ordering in liquid $Ti_{39.5}Zr_{39.5}Ni_{21}$ catalyzes the nucleation of a metastable icosahedral phase [46]. Significant stirring in the ground-based experiments may disturb this ordering, while it may persist under microgravity conditions. A recent study examined a coupling of nucleation events, measuring the delay time for a ferrite to austenite transition as a function of shear in a Fe-Cr-Ni stainless steel liquid [98]. Based on ground-based ESL and EML measurements and measurements in the microgravity environment of the ESA EML facility on the ISS, it was concluded that the observed delay time is due to a shear-enhanced retained driving free energy from the metastable ferrite phase. The coupled-flux model (Section 2.4) predicts that when the flow is reduced and long-range diffusion becomes dominant, the nucleation rate for phases with a different chemical concentration from that of the liquid should decrease. There is some experimental evidence for this in microgravity studies of the solidification of Al-Bi-Sn alloys [99]. A more recent study of a

$Zr_{57}Cu_{15.4}Ni_{12.6}Al_{10}Nb_5$ (Vit106), $Cu_{50}Zr_{50}$, and the quasicrystal-forming $Ti_{39.5}Zr_{39.5}Ni_{21}$ liquids showed that the maximum nucleation rate increased systematically with increased fluid flow in the liquids for Vit106, with compositional changes during crystallization, but stayed nearly unchanged for the other two, where the compositional changes were small [100]. To date, this is the best supporting evidence for the coupled-flux model for nucleation in the liquid; future studies on the ISS to improve the statistical significance of this result are planned.

7 Nucleation and Glass Formation

The key problem for glass formation is preventing significant nucleation and growth during the cooling of the liquid [101, 102]. For this reason, the earliest prediction for glass formation focused on liquid alloys with deep eutectics [101], since the temperature range over which nucleation could occur was small before the kinetics effectively froze out upon reaching the glass transition temperature. But in addition to the nucleation rate, the growth rate must also be considered. By combining these two rates, it becomes possible to determine the critical quenching rate for glass formation using a time-temperature-transformation (TTT) diagram, showing the times at a given temperature required to develop a certain volume fraction crystallization. A series of TTT diagrams fit to experimental data for Cu-Zr liquids of different compositions is shown in Fig. 7.10 [103]; the temperature is normalized to the liquidus temperature, T_l. The three diagrams show liquids of nearby concentration to the best glass-forming compositions, $Cu_{64}Zr_{36}$ (Fig. 7.10a), $Cu_{56}Zr_{44}$ (Fig. 7.10b), and $Cu_{50}Zr_{50}$ (Fig. 7.10c). If the cooling rate is sufficient to bypass the nose of the TTT curve, glass formation will result (shown schematically in Fig. 7.10b for illustration). The results of this study were that the effect of

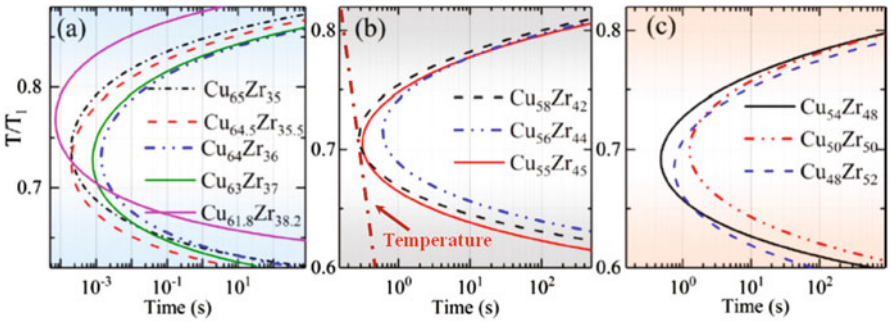

Fig. 7.10 The TTT diagrams for Cu-Zr alloys of different compositions normalized to the liquidus temperatures, T_l. Glass formation occurs if the temperature during cooling (illustrated by the solid dashed line in (**b**)) remains to the left of the nose of the TTT diagram. (Reprinted with permission from Ref. [103], copyright (2018), American Physical Society)

compositional change on glass-forming ability of the three best glasses differs, which had not been recognized before.

Recently, it has proven possible to do this in the microgravity environment of the ISS, constituting the first time that metallic glass production has been demonstrated in space [104]. Since metallic glasses are increasingly finding applications for specific needs, such as lubrication free gears for use in the cold environment of space [105], the ability to produce them in space or on other planets having a different gravitational environment could be very important.

Both nucleation and growth depend on the atomic mobility (generally estimated from the diffusion coefficient in the liquid) and the driving free energy. At high temperatures, the diffusion coefficient in the liquid can be related to the viscosity, using the Stokes-Einstein relation. The viscosity can be characterized by the fragility of the liquid [106], which is related to the temperature dependence of the viscosity in a normalized temperature plot (i.e., T/T_g where T_g is the glass transition temperature). Within the metallic glass community, fragility is often associated with glass formability [107], which is reasonable since glass formation hinges on avoiding crystal nucleation and growth. Stronger liquids are believed to be thermodynamically more stable than fragile ones and have larger viscosities at high temperatures, properties that will suppress the nucleation and growth of the crystal phases and make glass formation easier. However, there are exceptions to the link between fragility and glass-forming ability. Sorbitol and Salol, for example, are very fragile liquids that form glasses [108], and a recent study in metallic glasses showed that fragility alone did not give a good prediction of glass formability [109]; a better prediction was found there when using the fragility and reduced glass transition temperature. Using the fragility and glass transition temperature as a predictor of glass formability poses a problem, however, since the glass must first be prepared. A recent study found that these quantities can be calculated from properties of the high-temperature liquid, allowing a truly predictive model of glass formability from the perspective of nucleation and growth [110, 111].

8 Conclusions

In conclusion, there has been a recent resurgent interest and activity in the study of nucleation in liquid and glasses. There are new tools, such as containerless processing and the availability of the microgravity environment on the International Space Station, that are allowing nucleation to be probed more deeply. An increased computational power has led to more realistic simulations of nucleation processes. The results of these studies show that the thermodynamic model of the commonly used classical nucleation theory is inadequate for developing a quantitative understanding of the nucleation process. A key problem is that the interface between the nuclei of the new phase and the original phase is not sharp, but diffuse. However, there are now models that take this into account, and they are starting to be used to analyze nucleation data. Of greater consequence is the increasing realization that

nucleation involves multiple connected order parameters and that there can exist multiple nucleation pathways. The structure of the liquid or glass is also now seen to be important in the nucleation process. Clearly, a great deal more of study is needed to sort out these issues and to develop new models to treat them. Microgravity research has played and will continue to play an important role in deepening our understanding of nucleation processes.

Acknowledgments The preparation of this chapter was supported by the National Aeronautics and Space Administration (NASA) under grant NNX16AB52G and the National Science Foundation under grants DMR 1720296 and DMR 1904281.

References

1. K.F. Kelton, A.L. Greer, in *Nucleation in Condensed Matter – Applications in Materials and Biology*, Pergamon Materials Series, ed. by R. W. Cahn, 1st edn., (Elsevier, Amsterdam, 2010), p. 726
2. Z.L. Liu, Review of grain refinement of cast metals through inoculation: Theories and developments. Metall. Mater. Trans. A. Phys. Metall. Mater. Sci. **48A**, 4755–4776 (2017)
3. C.A. Angell, Glass formation and glass transition in supercooled liquids, with insights from study of related phenomena in crystals. J. Non-Cryst. Solids **354**, 4703–4712 (2008)
4. E.D. Zanotto, Glass crystallization research a 36-year retrospective. Part I, fundamental studies. Int. J. Appl. Glas. Sci. **4**, 105–116 (2013)
5. L.R. Pinckney, G.H. Beall, Microstructural evolution in some silicate glass-ceramics: A review. J. Am. Ceram. Soc. **91**, 773–779 (2008)
6. J.R. Cox, L.A. Ferris, V.R. Thalladi, Selective growth of a stable drug polymorph by suppressing the nucleation of corresponding metastable polymorphs. Ang. Chem. Int. Ed. **46**, 4333–4336 (2007)
7. S.D. Thakore, A. Sood, A.K. Bansal, Emerging role of primary heterogeneous nucleation in pharmaceutical crystallization. Drug Dev. Res. **81**, 3–22 (2020)
8. Y.S. You, T.Y. Kang, S.J. Jun, Control of ice nucleation for subzero food preservation. Food Eng. Rev. **13**, 15–35 (2021)
9. M.J.H. Akanda, M.R. Norazlina, F.S. Azzatul, S. Shaarani, H. Mamat, J.S. Lee, J. Norliza, A.H. Mansoor, J. Selamat, F. Khan, P. Matanjun, M.Z.I. Sarker, Hard fats improve the physicochemical and thermal properties of seed fats for applications in confectionery products. Food Rev. Int. **36**, 601–625 (2020)
10. K.B. Storey, J.M. Storey, Biochemical adaption for freezing tolerance in the Wood Frog, Rana Sylvatica. J. Comp. Physiol. B Biochem. Syst. Environ. Physiol. **155**, 29–36 (1984)
11. C. Cerini, S. Geider, B. Dussol, C. Hennequin, M. Daudon, S. Veesler, S. Nitsche, R. Boistelle, P. Berthezene, P. Dupuy, A. Vazi, Y. Berland, J.C. Dagorn, J.M. Verdier, Nucleation of calcium oxalate crystals by albumin: Involvement in the prevention of stone formation. Kidney Int. **55**, 1776–1786 (1999)
12. D.G. Fahrenheit, Experimenta et observationes de congelatione aquae in vacuo factae. Philos. Trans. R. Soc. **39**, 78–89 (1724)
13. D. Turnbull, Kinetics of solidification of supercooled liquid mercury droplets. J. Chem. Phys. **20**, 411–424 (1952)
14. J.W. Gibbs, *Scientific Papers*, vol I, II (Longmans Green, London, 1906)
15. M. Volmer, A. Weber, Keimbildung in übersättigten Gebilden. Z. Phys. Chem. **119**, 227–301 (1926)

16. R. Becker, W. Döring, Kinetic treatment of grain-formation in super-saturated vapours. Ann. Phys. **24**, 719–752 (1935)
17. D. Turnbull, J.C. Fisher, Rate of nucleation in condensed systems. J. Chem. Phys. **17**, 71–73 (1949)
18. L. Granasy, F. Igioi, Comparison of experiments and modern theories of crystal nucleation. J. Chem. Phys. **107**, 3634–3644 (1997)
19. L. Granasy, P.F. James, Nucleation in oxide glasses: comparison of theory and experiment. Proc. R. Soc. Lond. Ser. A (Math. Phys. Eng. Sci.) **454**, 1745 (1998)
20. C.K. Bagdassarian, D.W. Oxtoby, Crystal nucleation and growth from the undercooled liquid: A nonclassical piecewise parabolic free energy model. J. Chem. Phys. **100**, 2139–2148 (1994)
21. F. Spaepen, Homogeneous nucleation and the temperature dependence of the crystal-melt interfacial tension, in *Solid State Physics*, ed. by H. Ehrenreich, D. Turnbull, (Academic, New York, 1994), pp. 1–32
22. L. Gránásy, Diffuse interface theory of nucleation. J. Non-Cryst. Solids **162**, 301–303 (1993)
23. L. Granasy, Diffuse interface model of crystal nucleation. J. Non-Cryst. Solids **219**, 49–56 (1997)
24. L. Granasy, Diffuse interface approach to vapour condensation. Europhys. Lett. **24**, 121–126 (1993)
25. D. Van Hoesen, *Thermophysical Properties and Phase Transformations in Metallic Liquids and Silicate Glasses*. PhD thesis in Physics (Washington University in St. Louis, 2000)
26. H. Reiss, The kinetics of phase transitions in binary systems. J. Chem. Phys. **18**, 840–848 (1950)
27. D.T. Wu, Nucleation theory, in *Solid State Physics*, ed. by H. Ehrenreich, F. Spaepen, (Academic, Boston, 1997), pp. 37–187
28. K. Binder, D. Stauffer, Statistical theory of nucleation, condensation and coagulation. Adv. Phys. **25**, 343–396 (1976)
29. D. Stauffer, Kinetic theory of two-component ('heteromolecular') nucleation and condensation. J. Aerosol Sci. **7**, 319–333 (1976)
30. D.E. Temkin, V.V. Shevelev, On the theory of nucleation in two-component systems. J. Cryst. Growth **52**, 104–110 (1981)
31. K.C. Russell, Linked flux analysis of nucleation in condensed phases. Acta Metall. **16**, 761–769 (1968)
32. P.F. Wei, K.F. Kelton, R. Falster, Coupled-flux nucleation modeling of oxygen precipitation in silicon. J. Appl. Phys. **88**, 5062–5070 (2000)
33. H. Diao, R. Salazar, K.F. Kelton, L.D. Gelb, Impact of diffusion on concentration profiles around near-critical nuclei and implications for theories of nucleation and growth. Acta Mater. **56**, 2585–2591 (2008)
34. K.F. Kelton, Time-dependent nucleation in partitioning transformations. Acta Mater. **48**, 1967–1980 (2000)
35. S. Wonczak, R. Strey, D. Stauffer, Confirmation of classical nucleation theory by Monte Carlo simulations in the 3-dimensional Ising model at low temperature. J. Chem. Phys. **113**, 1976–1980 (2000)
36. V.A. Shneidman, K.A. Jackson, K.M. Beatty, On the applicability of the classical nucleation theory in an Ising system. J. Chem. Phys. **111**, 6932–6941 (1999)
37. W.C. Swope, H.C. Andersen, 106 particle molecular-dynamics studie of homogeneous nucleation of crystals in a supercooled atomic liquid. Phys. Rev. B **41**, 7042–7054 (1990)
38. J.K. Bording, J. Tafto, Molecular-dynamics simulation of growth of nanocrystals in an amorphous matrix. Phys. Rev. B **62**, 8098–8103 (2000)
39. J.K. Lee, J.A. Barker, F.F. Abraham, Theory and Monte-Carlo simulation of physical clusters in imperfect vapor. J. Chem. Phys. **58**, 3166–3180 (1973)
40. K. Dahlberg, A. Agrawal, R. Chang, Z. Nussinov, K.F. Kelton, private communication (2021)
41. F.C. Frank, A discussion on theory of liquids: Supercooling of liquids. Proc. R. Soc. Lond. Ser. A (Math. Phys. Eng. Sci.) **215**, 43–46 (1952)

42. P. Ganesh, M. Widom, *Ab initio* simulations of geometrical frustration in supercooled liquid Fe and Fe-based metallic glass. Phys. Rev. B. **77**, 014205 (2008)
43. T.T. Debela, X.D. Wang, Q.P. Cao, D.X. Zhang, J.Z. Jiang, The crystallization process of liquid vanadium studied by *ab initio* molecular dynamics. J. Phys. Condens. Matter **26**, 155101 (2014)
44. T.T. Debela, X.D. Wang, Q.P. Cao, Y.H. Lu, D.X. Zhang, H.-J. Fecht, H. Tanaka, J.Z. Jiang, Nucleation driven by orientational order in supercooled niobium as seen via ab initio molecular dynamics. Phys. Rev. B **89**, 104205 (2014)
45. T.T. Debela, X.D. Wang, Q.P. Cao, D.X. Zhang, J.Z. Jiang, Comparative study of crystallization process in metallic melts using ab initio molecular dynamics simulations. J. Phys. Condens. Matter **29**, 185401 (2017)
46. K.F. Kelton, G.W. Lee, A.K. Gangopadhyay, R.W. Hyers, T.J. Rathz, J.R. Rogers, M.B. Robinson, D.S. Robinson, First X-ray scattering studies on electrostatically levitated metallic liquids: demonstrated influence of local icosahedral order on the nucleation barrier. Phys. Rev. Lett. **90**, 195504 (2003)
47. T. Kawasaki, H. Tanaka, Formation of a crystal nucleation from liquid. Proc. Natl. Acad. Sci. U. S. A. **107**, 14036–14041 (2010)
48. J. Russo, H. Tanaka, The microscopic pathway tocrystallization in supercooled liquids. Sci. Rep. **2**, 505 (2012)
49. Z.G. Wang, C.H. Chen, S.V. Ketov, K. Akagi, A.A. Tsarkov, Y. Ikuhara, D.V. Louzguine-Luzgin, Local chemical ordering within the incubation period as a trigger for nanocrystasllization of a highly supercooled Ti-based liquid. Mater. Des. **156**, 504–513 (2018)
50. E. Cini, B. Vinet, P.J. Desre, A thermodynamic approach to homogeneous nucleation via fluctuations of concentration in binary liquid alloys. Phil. Mag. A **80**, 955–966 (2000)
51. M.E. McKenzie, B. Deng, D.C. Van Hoesen, X. Xia, D.E. Baker, A. Rezikyan, R.E. Youngman, K.F. Kelton, Nucleation pathways in barium silicate glasses. Sci. Rep. **11**, 69 (2021)
52. Y. Shibuta, S. Sakane, E. Miyoshi, S. Okita, T. Takaki, M. Ohno, Heterogeneity in homogeneous nucleation from billion-atom molecular dynamics simulation of solidification of pure metal. Nat. Commun. **8**, 10 (2017)
53. F. Puosi, A. Pasturel, Dynamic slowing-down and crystal nucleation in a supercooled metallic glass former induced by local icosahedral order. Phys Rev Mater **3**, 6 (2019)
54. Y.Q. Cheng, H.W. Sheng, E. Ma, Relationship between structure, dynamics, and mechanical properties in metallic glass-forming alloys. Phys. Rev. B **78**, 7 (2008)
55. L. Berthier, G. Biroli, Theoretical perspective on the glass transition and amorphous materials. Rev. Mod. Phys. **83**, 587–645 (2011)
56. F. Puosi, A. Pasturel, Nucleation kinetis in a supercooled metallic glass former. Acta Mater. **174**, 387–397 (2019)
57. D. Moroni, P.R. ten Wolde, P.G. Bolhuis, Interplay between structure and size in a critical crystal nucleus. Phys. Rev. Lett. **94**, 235703 (2005)
58. R.S. Aga, J.F. Morris, J.J. Hoyt, M. Mendelev, Quantitative parameter-free prediction of simulated crystal-nucleation times. Phys. Rev. Lett. **96**, 245701 (2006)
59. G.E. Norman, V.V. Pisarev, Molecular dynamics analysis of the crystallization of an overcooled aluminum melt. Russ. J. Phys. Chem. A **86**, 1447–1452 (2012)
60. S.C. Costa Pradoa, J.P. Rino, E.D. Zanotto, Successful test of the classical nucleation theory by molecular dynamic simulations of BaS. Comput. Mater. Sci. **161**, 99–106 (2019)
61. A.O. Tipeev, E.D. Zanotto, Nucleation kinetics in supercooled $Ni_{50}Ti_{50}$: Computer simulation data corroborate the validity of the Classical Nucleation Theory. Chem. Phys. Lett. **735**, 136749 (2019)
62. C.W. Morton, W.H. Hofmeister, R.J. Bayuzick, A.J. Rulison, J.L. Watkins, The kinetics of solid nucleation in zirconium. Acta Mater. **46**, 6033–6039 (1998)
63. W.H. Hofmeister, C.W. Morton, R.J. Bayuzick, Monte Carlo testing of the statistical analysis of nucleation data. Acta Mater. **46**, 1903–1908 (1998)

64. V. Skripov, Homogeneous nucleation in melts and amorphous films. Curr. Top. Mater. Sci. **2**, 327–378 (1977)
65. T. Schenk, D. Holland-Moritz, V. Simonet, R. Bellissent, D.M. Herlach, Icosahedral short-range order in deeply undercooled metallic melts. Phys. Rev. Lett. **89**, 075507 (2002)
66. D. Shechtman, I. Blech, D. Gratias, J.W. Cahn, Metallic phase with long-range orientational order and no translational symmetry. Phys. Rev. Lett. **53**, 1951 (1984)
67. M.E. Sellers, D.C. Van Hoesen, A.K. Gangopadhyay, K.F. Kelton, Maximum supercooling studies in $Ti_{39.5}Zr_{39.5}Ni_{21}$, $Ti_{40}Zr_{30}Ni_{30}$, and $Zr_{80}Pt_{20}$ liquids-Connecting liquid structure and the nucleation barrier. J. Chem. Phys. **150** (2019)
68. H. Tanaka, Bond orientational ordering in a metastable supercooled liquid: A shadow of crystallization and liquid-liquid transition. J. Stat. Mech. Theory Exp. **1–27** (2010)
69. D. Kashchiev, Solution of the non-steady state problem in nucleation kinetics. Surf. Sci. **14**, 209–220 (1969)
70. X. Xia, D.C. Van Hoesen, M.E. McKenzie, R.E. Youngman, O. Gulbiten, K.F. Kelton, Time-dependent nucleation rate measurements in $BaO{\cdot}2SiO_2$ and $5BaO{\cdot}8SiO_2$ glasses. J. Non-Cryst. Solids **525**, 119575 (2019)
71. X. Xia, D.C. Van Hoesen, M.E. McKenzie, R.E. Youngman, K.F. Kelton, Low-temperature nucleation anomaly in silicate glasses shown to be artifact in a $5BaO{\cdot}8SiO_2$ glass. Nat. Commun. **12**, 2026 (2021)
72. M.C. Weinberg, E.D. Zanotto, Re-examination of the temperature dependence of the classical nucleation rate: homogeneous crystal nucleation in glass. J. Non-Cryst. Solids **108**, 99–108 (1989)
73. A.S. Abyzov, V.M. Fokin, A.M. Rodrigues, E.D. Zanotto, J.W.P. Schmelzer, The effect of elastic stresses on the thermodynamic barrier for crystal nucleation. J. Non-Cryst. Solids **432**, 325–333 (2016)
74. V.M. Fokin, A.S. Abyzov, E.D. Zanotto, D.R. Cassar, A.M. Rodrigues, Crystal nucleation in glass-forming liquids: Variation of the size of the "structural units" with temperature. J. Non-Cryst. Solids **447**, 35–44 (2016)
75. A.S. Abyzov, V.M. Fokin, N.S. Yuritsyn, A.M. Rodrigues, J.W.P. Schmelzer, The effect of heterogeneous structure of glass-forming liquids on crystal nucleation. J. Non-Cryst. Solids **462**, 32–40 (2017)
76. D.R. Cassar, A.H. Serra, O. Peitl, E.D. Zanotto, Critical assessment of the alleged failure of the Classical Nucleation Theory at low temperatures. J. Non-Cryst. Solids **547**, 120297 (2020)
77. K.F. Kelton, A.L. Greer, Test of classical nucleation theory in a condensed system. Phys. Rev. **B38**, 10089–10092 (1988)
78. A.L. Greer, K.F. Kelton, Nucleation in lithium disilicate glass: A test of classical theory by quantitative modeling. J. Am. Ceram. Soc. **74**, 1015–1022 (1991)
79. M. Buchwitz, R. Adlwarth-Dieball, P.L. Ryder, Kinetics of the crystallization of amorphous Ti_2Ni. Acta Metall. Mater. **41**, 1885–1892 (1993)
80. F.X. Bai, J.H. Yao, Y.X. Wang, J. Pan, Y. Li, Crystallization kinetics of an Au-based metallic glass upon ultrafast heating and cooling. Scr. Mater. **132**, 58–62 (2017)
81. K. Kosiba, S. Scudino, R. Kobold, U. Kühn, A.L. Greer, J. Eckert, S. Pauly, Transient nucleation and microstructural design in flash-annealed bulk metallic glasses. Acta Mater. **127**, 416–425 (2017)
82. A. Penkova, W. Pan, F. Hodjaoglu, P.G. Vekilov, Nucleation of protein crystals under the influence of solution shear flow. Ann. N. Y. Acad. Sci. **1077**, 214–231 (2006)
83. J.A. Baird, D. Santiago-Quinonez, C. Rinaldi, L.S. Taylor, Role of viscosity in influencing the glass-forming ability of organic molecules from the undercooled melt state. Pharm. Res. **29**, 271–284 (2012)
84. A.A. Chernov, Protein crystals and their growth. J. Struct. Biol. **142**, 3–21 (2003)
85. M.R. Meier, L. Lei, A. Rinkenburger, J. Plank, Crystal growth of Ca3Al(OH)(6)·12H(2)O (2)·(SO4)(3)·2H(2)O (Ettringite) studied under microgravity conditions. J. Wuhan Univ. Technol. Mater. Sci. Ed. **35**, 893–899 (2020)

86. X.Y. Liu, K. Tsukamoto, M. Sorai, New kinetics of $CaCO_3$ nucleation and microgravity effect. Langmuir **16**, 5499–5502 (2000)
87. A. Tsuchida, E. Takyo, K. Taguchi, T. Okubo, Kinetic analyses of colloidal crystallization in shear flow. Colloid Polym. Sci. **282**, 1105–1110 (2004)
88. A. Penkova, W.C. Pan, F. Hodjaoglu, P.G. Vekilov, Nucleation of protein crystals under the influence of solution shear flow, in *Interdisciplinary Transport Phenomena in the Space Sciences*, ed. by S. S. Sadhal, (Wiley-Blackwell, Hoboken, 2006), pp. 214–231
89. C. Forsyth, P.A. Mulheran, C. Forsyth, M.D. Haw, I.S. Burns, J. Sefcik, Influence of controlled fluid shear on nucleation rates in glycine aqueous solutions. Cryst. Growth Des. **15**, 94–102 (2015)
90. R. Blaak, S. Auer, D. Frenkel, H. Lowen, Crystal nucleation of colloidal suspensions under shear. Phys. Rev. Lett. **93**, 068303 (2004)
91. A.V. Mokshin, B.N. Galimzyanov, J.L. Barrat, Extension of classical nucleation theory for uniformly sheared systems. Phys. Rev. E **87**, 062307 (2013)
92. D. Richard, T. Speck, The role of shear in crystallization kinetics: From suppression to enhancement. Sci. Rep. **5**, 7 (2015)
93. F. Mura, A. Zaccone, Effects of shear flow on phase nucleation and crystallization. Phys. Rev. E **93**, 11 (2016)
94. W.H. Hofmeister, R.J. Bayuzick, R. Hyers, G. Trapaga, Cavitation-induced nucleation of zirconium in low earth orbit. Appl. Phys. Lett. **74**, 2711–2713 (1999)
95. D.M. Herlach, S. Burggraf, P. Galenko, C.A. Gandin, A. Garcia-Escorial, H. Henein, C. Karrasch, A. Mullis, M. Rettenmayr, J. Valloton, Solidification of undercooled melts of Al-based alloys on Earth and in space. JOM **69**, 1303–1310 (2017)
96. S.H. Oh, Y. Kauffmann, C. Scheu, W.D. Kaplan, M. Ruhle, Ordered liquid aluminum at the interface with sapphire. Science **310**, 661–663 (2005)
97. A.L. Greer, Liquid metals: Supercool order. Nat. Mater. **5**, 13–14 (2006)
98. D.M. Matson, Retained free energy as a driving force for phase transformation during rapid solidification of stainless steel alloys in microgravity. npj Microgravity **4**, 6 (2018)
99. H.X. Jiang, S.X. Li, L.L. Zhang, J. He, J.Z. Zhao, Effect of microgravity on the solidification of aluminum-bismuth-tin immiscible alloys. npj Microgravity **5**, 9 (2019)
100. A.K. Gangopadhyay, M.E. Sellers, G.P. Bracker, D. Holland-Moritz, D.C. Van Hoesen, S. Koch, P.K. Galenko, A.K. Pauls, R.W. Hyers, K.F. Kelton, Demonstration of the effect of stirring on nucleation from experiments on the International Space station. npj Microgravity, **7**, 31 (2021)
101. D. Turnbull, Under what conditions can a glass be formed? Contemp. Phys. **10**, 473–488 (1969)
102. H. Fecht, W.L. Johnson, Thermodynamic properties and metastability of bulk metallic glasses. Mater. Sci. Eng. A-Struct. Mater. Prop. Microstruct. Process. **375**, 2–8 (2004)
103. S. Ganorkar, S. Lee, Y.H. Lee, T. Ishikawa, G.W. Lee, Origin of glass forming ability of Cu-Zr alloys: A link between compositional variation and stability of liquid and glass. Phys Rev Mater **2**, 115606 (2018)
104. M. Mohr, R.K. Wunderlich, D.C. Hofmann, H.J. Fecht, Thermophysical properties of liquid $Zr_{52.5}Cu_{17.9}Ni_{14.6}Al_{10}Ti_5$ – prospects for bulk metallic glass manufacturing in space. npj Microgravity **5**, 8 (2019)
105. https://www.space.com/34890-metallic-glass-ideal-for-space-mission-gears.html
106. C.A. Angell, *Strong and Fragile Liquids. in Relaxation in Complex Systems* (National Technical Information Service, U.S. Department of Commerce, Springfield, 1984)
107. R. Busch, E. Bakke, W.L. Johnson, Viscosity of the supercooled liquid and relaxation at the glass transition of the $Zr_{46.76}Ti_{8.25}Cu_{7.5}Ni_{10}Be_{27.5}$ bulk metallic glass forming alloy. Acta Mater. **46**, 4725–4732 (1998)

108. R. Böhmer, K.L. Ngai, C.A. Angell, D.J. Plazek, Nonexponential relaxations in strong and fragile glass formers. J. Chem. Phys. **99**, 4201–4209 (1993)
109. W.L. Johnson, J.H. Na, M.D. Demetriou, Quantifying the origin of metallic glass formation. Nat. Commun. **7**, 10313 (2016)
110. R. Dai, R. Ashcraft, A.K. Gangopadhyay, K.F. Kelton, Predicting metallic glass formation from properties of the high temperature liquid. J. Non-Cryst. Solids **525**, 119673 (2019)
111. R. Dai, A.K. Gangopadhyay, R.J. Chang, K.F. Kelton, A method to predict the glass transition temperature in metallic glasses from properties of the equilibrium liquid. Acta Mater. **172**, 1–5 (2019)